International Journal of Heat and Mass Transfer 53 (2010) 3414–3428

Contents lists available at ScienceDirect

International Journal of Heat and Mass Transfer

journal homepage: www.elsevier.com/locate/ijhmt

Performance of naphthalene thermosyphons with non-condensable gases – Theoretical study and comparison with data

Marcia Barbosa Henriques Mantelli [a,*], Wagner Barbosa Ângelo [b], Thomaz Borges [a]

[a] Heat Pipe Laboratory – LABTUCAL, Mechanical Engineering Department, Federal University of Santa Catarina, Campus Universitário Trindade, 88040-900 Florianópolis/SC, Brazil
[b] Petrobras, E&P/US-SUB/SGO, Rod. Amaral Peixoto 11.000, 27.925.290 Macaé/RJ, Brazil

ARTICLE INFO

Article history:
Received 17 July 2009
Received in revised form 20 February 2010
Accepted 20 February 2010
Available online 22 April 2010

Keywords:
Thermosyphons
Naphthalene thermosyphons
High temperature heat exchangers
Non-condensable gases (NGC)

ABSTRACT

Naphthalene thermosyphons are efficient heat transfer devices that operate within 250 and 400 °C. There is a lack of literature about naphthalene thermosyphons, especially with the presence of non-condensable gases (NCG). Thermal circuit resistance models, considering or not NCG, are developed. NCG–vapor flat front hypothesis is adopted. Condensation and evaporation heat transfer coefficients are obtained from literature correlations. Thermal resistance data provided from naphthalene thermosyphon charged with argon, is obtained using especial experimental setup. Two combinations of correlations provided good comparison with data, for thermosyphons with and without NCG. These models are successfully applied for heat exchanger design.

1. Introduction

Two-phase thermosyphons are high conductance thermal devices, which can present different geometries and sizes, being very suitable for applications in compact and efficient heat exchangers. Actually, the industry interest in such devices is increasing, as they are reliable, robust and safe and demands low maintenance.

Basically, a thermosyphon is a hollow evacuated tube, partially filled with working fluid. Heat is delivered to the thermosyphon in the bottom of the tube, the evaporator. The liquid in contact with the heat evaporates and the resulting vapor, due to the pressure gradients, flows to the top of the tube. In this region, the condenser, heat is removed and the vapor condensates. The resulting liquid returns to the evaporator by means of gravity. Thermosyphons and heat pipes are very similar devices; in heat pipes the liquid is returned to the evaporator by means of the capillary forces provided by a wick usually located close to the tube wall.

The heat Pipe Laboratory of the Federal University of Santa Catarina, Brazil (Labtucal/UFSC) has, over the past 15 years, developed several heat pipe and thermosyphon technology thermal equipment, for different industrial or electronic cooling applications. The research and development work includes: modeling and tests of special heat pipes or thermosyphons; testing of small scale equipment prototypes; design and fabrication of very small devices, for electronic thermal control of earth and satellite equipment [1–3]; design of large equipment, such as heating systems for industrial ovens [4,5] or asphalt storage tanks [6]; fabrication and test of cryogenic heat pipes, for cooling satellites sensors [7,8]; and high temperature thermosyphons [9].

Many of these equipment works at moderate temperature levels (between 0 and 250 °C). Water has been used as the working fluid. However, new industrial applications demands for higher operating temperature levels, ranging between 200 and 400 °C, where water is not appropriated. Actually, the water vapor pressure for temperatures above 250 °C, is very high, and, to guarantee the mechanical integrity of water thermosyphons operating at high temperatures, the case walls must be thick, increasing the equipment weight and cost. On the other hand, for very high temperature levels (above 600 °C), liquid metals, such as mercury and sodium are used, as reported in the literature [10,11]. For intermediate temperatures, between 300 and 600 °C, organic working fluids and, among them, naphthalene, has being considered as a suitable fluid [12–14] and has been applied in many heat exchangers in China. Although used naphthalene is hardly mentioned in classical books [15–18]. Naphthalene can chemically react with the case metal, generating non-condensable gases (NCG), which accumulate on the extreme condenser regions, reducing the heat transfer capacity of the thermosyphon. Not many theoretical and experimental works deal with the thermal performance of naphthalene thermosyphons, especially those concerning the presence of NCG.

Heat pipe or thermosyphon heat exchangers have been designed, tested and are operating in many countries around the world [14,19,20]. A software for the thermal design of these equip-

* Corresponding author. Tel.: +55 48 32342161x214; fax: +55 48 3721 9937x228.
E-mail addresses: marcia@emc.ufsc.br (M.B.H. Mantelli), wagnerangelo@petrobras.com.br (W.B. Ângelo), tborges@emc.ufsc.br (T. Borges).

0017-9310/$ - see front matter © 2010 Elsevier Ltd. All rights reserved.
doi:10.1016/j.ijheatmasstransfer.2010.03.041

Nomenclature

A	tube cross section area (m^2)
d	diameter (m)
h	coefficient of heat transfer (W/m^2 K)
H	condenser length (m)
K	thermal conductivity (W/m K)
l	length (m)
N	number of moles
P	pressure (Pa)
R	thermal resistance (°C/W)
$\Re$	ideal gas constant
T	temperature (°C, K)

Subscripts

0	initial condition
adiab	adiabatic
c	cross section
cond	condensation
eff	effective
env	environment
evap	evaporator
ext	external
f	fluid
int	internal
max	maximum
NCG	non-condensable gas
pc	cooling system wall
pool	pool
v	vapor
w	wall
water	water

ment was developed by Borges et al. [21], which takes into account the thermal resistances associated with the evaporation and condensation phenomena that happens inside the thermosyphon and the convection heat transfer that happens outside the evaporator and condenser section of the device. The coefficients of heat transfer used to estimate the thermosyphon internal evaporation and condensation resistances are obtained from literature correlations, which are based on experimental data, usually developed for working fluids such as water, alcohols, ammonia, etc. For the determination of outside thermosyphon convection heat transfer, literature correlations for cross flow tube bundle arrays [22] are applied. Actually, the thermal resistances associated with the external heat transfer mechanisms are usually much larger than the internal resistances. Therefore, the geometry and the number of thermosyphons are much more dependent on the capacity of the thermosyphon tube bundle to absorb and reject heat in the evaporator and condenser regions then the capacity of the tubes to transfer this heat. In these softwares, the overall internal thermosyphon resistance is estimated using the analogy between electrical and thermal circuit [23] models. These models present very good results for water, methanol, acetone and other well known working fluids. But almost no comparison of traditional models with moderate–high temperature working fluids, such as naphthalene, is found in the literature.

The influence of NCG in the thermal performance of thermosyphons is very important information to be considered for the design of heat exchangers. NCG results from deficiencies in the fabrication process (low vacuum inside the tube before charging, gasses or impurities dissolved in the working fluid, etc.) or due to the chemical reaction of the working fluid and case material.

Several theoretical models for the prediction of heat transfer behavior of heat pipes and thermosyphons can be found in the literature. Some of them take into account the presence of NCG. The level of complexity of these models varies from simple (electric analogy) to sophisticated two dimensional models, which considerers the presence of a non-flat vapor–NCG front in the condenser, usually solved using numerical methods. Obviously the complex models describe the physical phenomena with greater precision than the simple ones, but they are far more computational time consuming, being in many applications unsuitable for implementation in heat exchanger design softwares.

The main objective of the present paper is to study theoretical and experimentally the thermal performance of naphthalene thermosyphons, operating in several temperature levels, without and with the presence of NCG. Data obtained from an especial experimental apparatus, able to control simultaneously the heat power input and the thermosyphon temperature, are compared with the present model. The thermal behavior of this experimental apparatus is also modeled. Therefore, the present paper addresses the question of whether literature models developed for and compared with conventional working fluids can also be applied to naphthalene thermosyphons, with or without NCG. For the present study, a simple 1D model, based on the electric/thermal analogy, applicable to heat exchanger design softwares, is developed for the prediction of the thermal behavior of naphthalene thermosyphons.

2. Literature review

2.1. Thermosyphon modeling

The electrical and thermal analogy model has been widely applied for steady state conditions [18,23,24] in thermosyphons. Many papers in the literature study the condensation and evaporation processes inside thermosyphon condensers and evaporators. Most of the condensers theoretical works are based on the Nusselt classical model for vapor condensation over a vertical wall [25]. Two different regions are observed in the evaporator: the thin film and the pool. For the film region, models based on Nusselt evaporation, similar to those used for the condenser, were developed [26]. For the pool region, pool boiling evaporation theory is applied [25]. The models are compared with data and, as a result, model based correlations were obtained, which are used for the prediction of the coefficients of heat transfer for the evaporation and condensation inside the thermosyphon. Most of the experimental data used for correlations are based on water, but working fluids such as alcohols, ammonia and acetone were also tested. These models and correlations were implemented in the software developed for the design of heat exchangers [20,21], which has been used successfully for water thermosyphon equipment.

Although the condenser region plug effect of NCG in heat pipes and thermosyphons are similar, the condensation heat transfer phenomena are quite different for both devices, so that models developed for heat pipes cannot be directly applied for thermosyphons. The presence of NCG inside heat pipes was investigated along the years, mainly for the study of the thermal behavior of variable conductance heat pipes, which are usually applied for the thermal control of spacecrafts and satellites [15–18].

Edwards and Marcus (1972) [27] developed a 1D model for the prediction of the heat transfer in heat pipes with NCG. They observed that, in steady state conditions, there is a smooth decrease

in the vapor concentration and a correspondent increase in NCG concentration that occurs over an appreciable length of the pipe. Also, natural convection and tube wall axial conduction can influence this vapor/NCG front. They concluded that the flat-front theory applied for traditional variable conductance heat pipe, adopted as the physical model by Marcus and Fleishman (1970) [28] does not predict the front behavior very well. Edwards and Marcus tested heat pipes made of the following casing materials: stainless steel, titanium, nickel or aluminum, charged with: methanol, ammonia or water. They verified that the conductivity of the pipe wall has strong influence in the transition region between vapor and NCG. They used, for the Fourier law conduction models, the thermal effective conductivity concept, which includes the thermal conductivity of the working fluid and of the wick material. The theoretical results compared quite well with the data they obtained. Rohani and Tien, in 1973 [29], developed a steady two-dimensional heat and mass transfer numerical analysis in the vapor–NCG region of a gas loaded heat pipe. They applied their model to the following combination of vapor–NCG: water–nitrogen, methanol–nitrogen, ammonia–nitrogen, sodium–argon and water–air.

Later, in the 1980 decade, Tien and co-workers [30–32] developed more detailed theoretical and experimental studies for thermosyphons with NCG. Hijikata et al. (1984) [30] considered that, in addition to the axial mass diffusion, the radial diffusion caused NCG to accumulate at the vapor–liquid interface, retarding vapor condensation. They developed a 2D model applied for water thermosyphons with air as NCG. The vapor–gas mixture was assumed to follow the ideal gas law and the NCG are assumed stationary at the top of the condenser region. The wall condensation is assumed to follow the Nusselt type solution. The problem was solved numerically. Later, Peterson and Tien (1989) [32] established three levels of complexity for the theoretical treatment of the vapor–NCG front analysis: flat front, simplified analytical formulation and numerical calculations, which take into account the mass diffuse transport in the vapor–NCG interface region. They solved the 2D problem using the integral technique, which required, according to the authors, less computational time for the same result precision obtained by the Hijikata et al. They compared favorably their theoretical results with data that these same authors obtained for water in the presence of combination of the following NCGs: helium, neon and argon [31].

Another analytical model was presented and solved numerically in 1992 by Juxiang and Tongming [33], who claimed the development of a model which takes into account all the main factors that influence the gas distribution in the condenser of a gas-loaded thermosyphon. Also, an experimental work on water and N_2 thermosyphon was performed, presenting good comparison with the model. Maezawa and Ishihara, in 1994 [34] developed a simplified model which considered laminar filmwise condensation based on Nusselt theory and planar vapor/NCG front. They compared quite well their theoretical results with experimental data obtained for acetone and N_2. Other combination of working fluid (acetone, water, ethanol) and NCG (N_2, air and argon) were also studied. Zhou and Collins, in 1995 [35], presented a theoretical study for a gas-loaded thermosyphon, where the diffusion equation in the interface region was solved numerically. They also presented an experimental work where they performed accurate measurements of the thickness of the water condensed film. In 1999, Hashimoro et al. [36] presented an experimental study of the condensation characteristics of a NCG loaded thermosyphon, using water and air. They also employed a flat front model for the vapor–NCG front, in their numerical modeling.

Obviously, the 2D complete models describes better the physical behavior of the vapor–NCG front, but, on the other hand, are computational time consuming and, therefore, are not adequate to be implemented in softwares used for the design of thermosyphon heat exchangers. Flat front models, although very simple and less precise, are still successfully used for these applications. It is important to remember that there is a lack of studies which includes the comparison between the thermal behavior of naphthalene thermosyphons and theoretical models in the literature.

It is also important to note that Kaiping and Renz, in 1991 [37] in their study about the thermal diffusion effects between the vapor and the NCG front in turbulent partial condensation, demonstrated numerical and experimentally that, for a mixture of two gases which present high molecular mass difference, the thermal diffusion effect will be of importance. They tested mixtures of air and water vapor (molecular mass ratio of 1.6) and of iso-octane and N_2 (molecular mass ratio of 8.2) and concluded that the thermal diffusion for the first binary mixture was not important, but it was relevant for the second one. The ratio of molecular mass for naphthalene and air is 4.4, so the models developed for thermosyphons with NCG available in the literature, which do not take thermal diffusion (only mass diffusion) into consideration, might not be appropriate for naphthalene/air thermosyphons.

2.2. The naphthalene as a working fluid

Naphthalene is an aromatic hydrocarbon ($C_{10}H_8$) with molecular mass of 128.16 g/ml. Detailed characteristics of the naphthalene can be found in the work of Bruce et al. [38]. Vapor pressure is one of the most important parameters to be considered in the selection of the appropriated thermosyphon and heat pipe working fluid. Fig. 1 presents the vapor pressure as a function of the condensation temperature for the naphthalene and for the water, for comparison. It can be observed that the naphthalene vapor pressure is more than one order of magnitude lower than that of the water, being, therefore, more appropriated for thermosyphons operating at higher temperature levels.

More recently, Devarakonda and Anderson [39], in 2005, proposed the use of several working fluids, which present low vapor pressure for operating at the temperature range from 127 to 427 °C: aniline, naphthalene, toluene, hydrazine and phenols. They also stated that the heat pipe technology is mature for low and high temperature levels, but for intermediate temperatures, research still needs to be done. They suggested that the working temperature should be around 100 °C below the working fluid critical point.

Anderson [40], in 2007, presented a study of intermediate temperature fluids for heat pipes and loop heat pipes. This

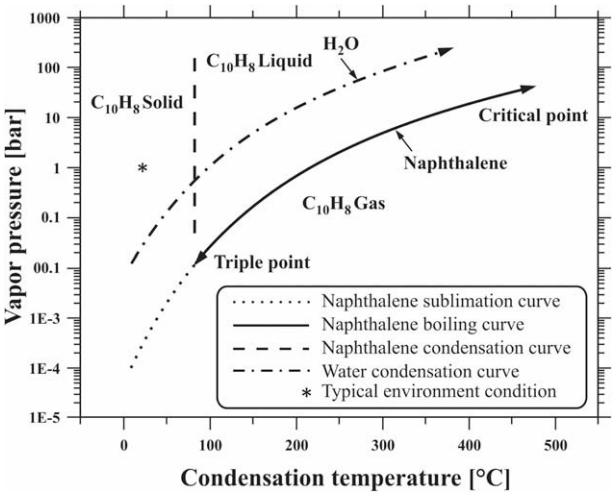

Fig. 1. Vapor pressure as a function of the temperature for naphthalene and water.

researcher performed a 5520 h life test of a carbon steel–naphthalene thermosyphon at 350 °C. He showed that the naphthalene did not degrade (did not produce considerable amount of NCG), concluding, therefore, that naphthalene and carbon steel are compatible. In this same paper, Anderson states that naphthalene is compatible with stainless steel, nickel–cooper alloys and titanium, for operating temperatures above 320 °C. For low temperature levels, the naphthalene demonstrated to be compatible with aluminum and low-alloy carbon steel. Also, naphthalene showed to be compatible with stainless steel for high temperatures (380 °C), in short period tests. Anderson [40] also believes that the fluoride composites are more stable than hydrogen composites, but this observation still needs life tests confirmation.

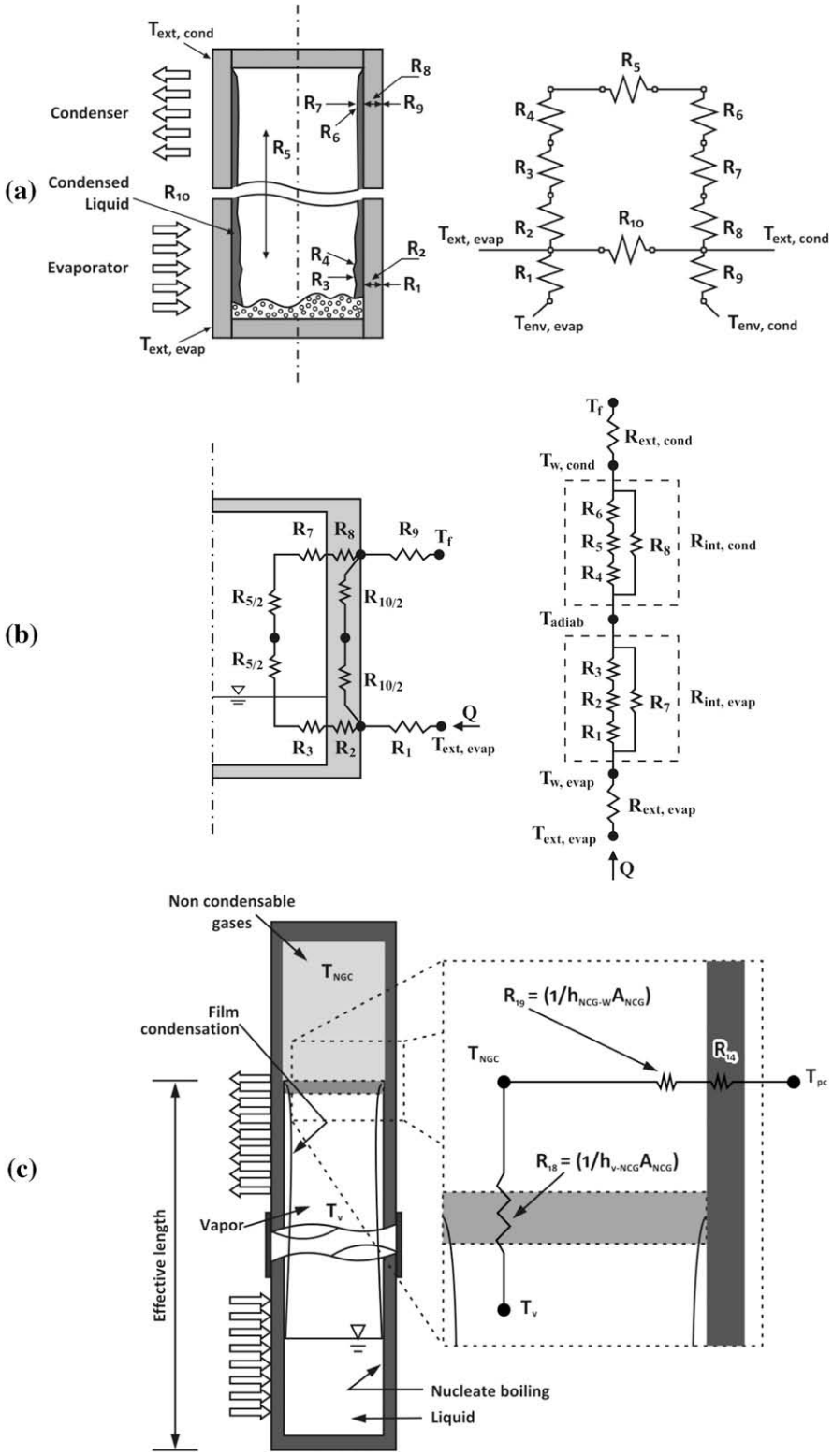

Fig. 2. Thermosyphon thermal circuits. (a) Typical, according to Mantelli et al. [24]. (b) Adopted in the present work. (c) Detail showing the internal thermal resistances.

3. Analytical models

The analogy between electric and thermal circuit model is usually applied for thermosyphons operating in steady state conditions [18,23]. A typical thermal circuit [23,24] is presented in Fig. 2 for thermosyphons operating without NCG. The thermal resistances are defined as the ratio between temperature differences and the heat power transferred. In this figure, R_1 and R_9 are related to the external heat exchange phenomena; R_2, R_8 and R_{10} are related to the heat conduction through the tube wall in the axial (evaporator and condenser regions) and longitudinal directions, respectively; R_3 is related to the evaporation, and has two sub regions: the pool boiling resistance, in the evaporator rear region where working fluid accumulates, and the liquid film in the wall; R_4 and R_6 are the thermal resistances associated with the interface liquid–vapor, for the evaporator and condenser, respectively, usually neglected; and, finally, R_5 is the thermal resistance associated with the vapor flow inside the tube. The resistances associated with the condensation and evaporation phenomena are determined with the use of correlations obtained from the literature, as presented by Mantelli et al. [24].

The left side of Fig. 2b presents the schematic of the thermal circuit adopted, where the resistances are the same presented in Fig. 2a, but, in the right side, the original circuit is slightly simplified, with the application of the hypothesis that the wall temperature is the same of the vapor temperature in the adiabatic section of the thermosyphon. With this simplification, it is possible to model the evaporator and the condenser sections separately.

The left side of Fig. 2c presents a sketch of the physical model adopted for a naphthalene stainless steel thermosyphon operating in vertical position, considering the presence of NCG inside the thermosyphon. In this model, all the length of the evaporator is considered full of working fluid. The evaporation happens in nucleate pool boiling regime. No external heat transfer is considered for the adiabatic section, which is insulated. The condensation happens below the NCG layer, located in the condenser. The vapor–NGC front is considered flat and no mass or thermal diffusion is considered. The two-phase flow is annular; the liquid flows from condenser to evaporator over the internal surface of the tube, while the vapor runs in countercurrent flux, in the central region of the tube. Natural convection heat transfer is considered for the NCG condenser region.

Other hypothesis are also adopted: steady sate conditions; uniform film condensation over the inside wall of the tube; naphthalene is a Newtonian fluid; there is no significant chemical reaction during the thermosyphon operation; all heat transfer processes are one-dimensional; the vapor drag of small condensate drops is neglected; the convective boiling of the liquid film in the upper regions of the evaporator wall is also neglected and no variation of physical–chemical properties are considered.

The calorimeter used to extract heat from the thermosyphon during tests is also modeled using the thermal and electrical analogy. To control the power input and the thermosyphon temperature level, a thin layer of static air fills the cavity between the tube wall and the condenser water jacket, where heat is removed from the system. Simple classic convection heat transfer theory [41] shows that no convection is expected through the static air in the gap. Therefore, heat is transferred by pure conduction. In the top of Fig. 3, the thermal resistance circuit associated with the condenser is presented. In Fig. 3 Detail A, R_{11} and R_{12} represent the resistances between the air and thermosyphon and between air and cooling system walls, respectively. R_{13} represents the radiation thermal resistance between the cavity walls. In the present case, R_{11}, R_{12} and R_{13} were all joined in one unique thermal resistance equivalent to the conduction through the air, considered static.

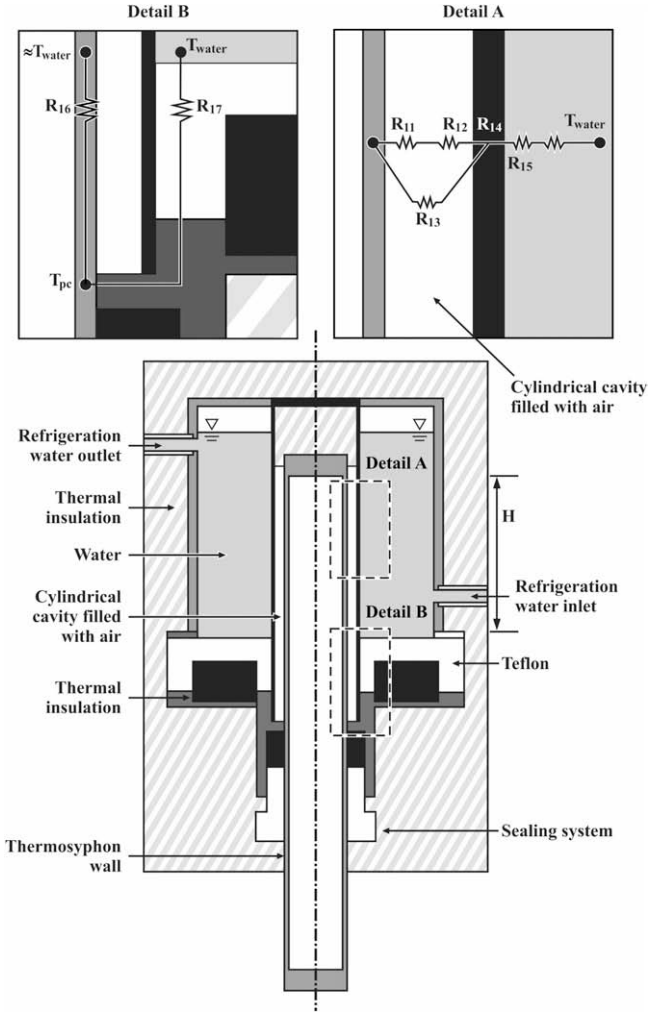

Fig. 3. Sketch of the experimental heat removal system and the associated thermal circuit.

R_{14} is associated with the conduction heat transfer of the cooling system internal wall, R_{15} the cooling water convection resistance, determined using literature well known convection heat transfer coefficients. In Detail B, R_{16} is the conduction thermal resistance in the axial direction of the thermosyphon wall and finally R_{17} represents the conduction resistance of the insulation material in the adiabatic section, which is parallel to R_{16}. Also in this figure, H is the length of the condenser, T_{pc} is the cooling system wall temperature and T_{water} is the temperature of the refrigeration water. All the conduction heat transfer resistances are determined using classical Fourier law expressions (see following section).

The heat transfer limits (flooding, sonic, boiling, etc.) for thermosyphons were calculated by Ângelo [42] using the models available in the literature [18]. All the heat transfer limits were far beyond the power input of the present study and will not be presented in this paper.

3.1. Models for the thermosyphon thermal resistances

Well known equations are used to determine the wall conduction radial resistances and the convection resistances [22], associated with the thermal circuits presented in Section 2. The main challenge is to determine the coefficients of heat transfer.

As reported in the literature [9,11,42], the thermal performance of high temperature thermosyphons depends strongly of the heat

transfer mechanisms inside the evaporator. According to the heat transfer regime in this region, different correlations can be used to estimate the heat transfer rate. In the present case, nucleate pool boiling is assumed. Angelo [42] verified that the experimental heat fluxes used in the present work are well below those needed to reach boiling crisis (critical flux), but are high enough to keep the thermosyphon operation in nucleate boiling regime. Many correlations are available to evaluate the onset of nucleate boiling. Using a model developed by Kamil et al. [43], Angelo [42] determined that, for the naphthalene, the onset fluxes for nucleate boiling varied between 11 and 1500 W/m^2, below 5600 W/m^2, the smallest heat flux experimentally tested, showing that the nucleate boiling hypothesis is suitable for the present model.

As already mentioned, the evaporator and pool lengths are considered equal ($l_{pool} = l_{evap}$). This is a good approximation, as the evaporator filling ratio (ratio between the volumes of the working fluid and the evaporator) of the thermosyphon studied is 80% and, during operation, the bubbles formed in the pool increases the effective length of the working fluid in the evaporator.

Four correlations: Foster and Zuber [25], Kutatelaze [25], Stephan and Abdelsalam [44] and Cooper [45], were used to estimate the evaporator coefficient of heat transfer (nucleate pool boiling), for the thermosyphon under investigation. Fig. 4a shows plots of these coefficients as a function of the vapor temperature, considering the conditions of 100%, 50% and 10% of the maximum theoretical heat flux that the apparatus, where the tests were conducted, is able to transfer. The apparatus heat transfer capacity was used in this study, as the thermosyphon power limits shows that this device is able to transfer far beyond the 100% of the setup maximum power. One can see that the variation of the coefficient heat transfer values is large (one or two orders of magnitude) for the different correlations used and for the heat power input. As already observed in this paper, none of these correlations were developed for organic fluids such as naphthalene.

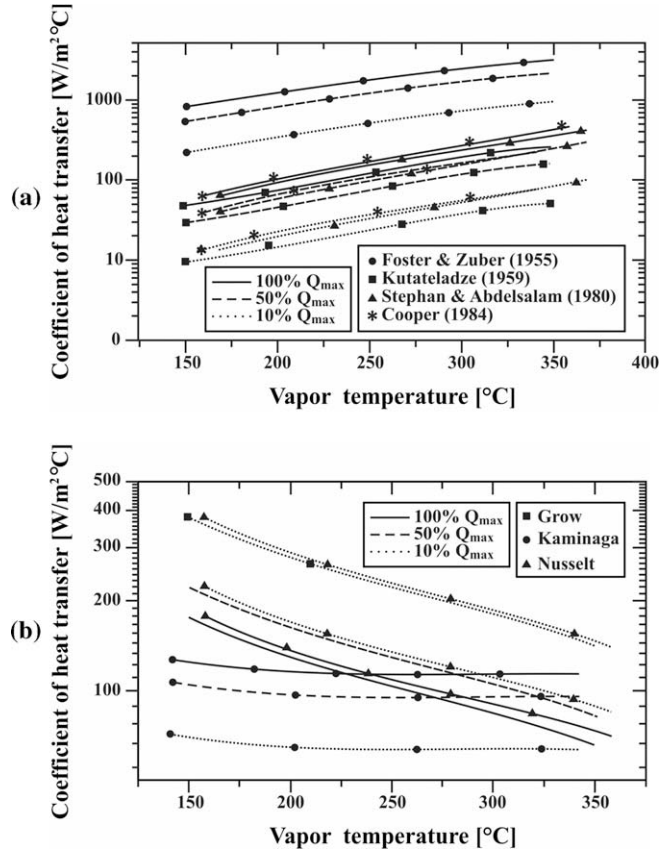

Fig. 4. Coefficients of heat transfer for three conditions of the maximum heat transfer capacity of the experimental apparatus. (a) Pool nucleate boiling. (b) Film condensation, for condenser active part.

It is important to note that the thermodynamic and heat transport properties of naphthalene are not well known, especially for the saturated conditions. Also, when the distance between gas molecules is large when compared to the container dimensions, the hypothesis of continuum, usually applied to many models available in the literature, are not valid. This situation may happen during the start up of naphthalene thermosyphons, when vacuum conditions at room temperature are observed. It is well known in the literature that, when the Knudsen number (defined as the ratio between the mean free path distance among molecules and a characteristic dimension of the container) is larger than 0.01, the continuum hypothesis is valid. Angelo [42] conducted a study of the naphthalene thermosyphons for tubes of more than 10 mm of diameter and concluded that, for temperature levels above 30 °C, the continuum hypothesis is valid for naphthalene.

The coefficient of heat transfer associated with the active part of the condenser, not blocked by the NCG, is evaluated by means of three correlations for film condensation (Groll and Rosler, Kaminaga and Nusselt), following the conclusions of Mantelli et al. [24], who compared several models. Fig. 4b shows the plot of the heat transfer coefficients as a function of the vapor temperature, for these three correlations and for three conditions of experimental setup heat input capacities: 100%, 50% and 10%. This figure shows that the heat transfer coefficients obtained by the correlation of Nusselt can be four times larger than that obtained by Kaminaga, for low temperature levels. The behaviors of the Nusselt and Groll correlations are similar, while the Kaminaga's correlation does not follow the same trends, presenting almost constant values for all temperature levels studied. The same observation made for the evaporator is valid here: the correlations employed were not developed for organic fluids such as naphthalene.

It is well known that NCG accumulate at the upper region of the condenser section in vertical thermosyphons and that this region does not transfer heat effectively. Therefore, it is possible to define an effective thermosyphon operation length l_{eff} (see Fig. 2c), which corresponds to the thermosyphon length where there is effective heat transfer.

The effective length of the thermosyphon can be determined if the amount of NCG (mass) inside a thermosyphon is known. The pressure is assumed to be that of the vapor for the thermosyphon operating temperature. Using the ideal gas law, it is possible to determine the volume of the NCG, and therefore, the length this gas occupy inside the tube. Then, the NCG length is given by

$$l_{NCG} = \frac{1}{A_c}\frac{N_0 \Re T_{NCG}}{P_{NCG}}, \tag{1}$$

where A_c is the tube cross section area, N_0 is the number of moles, T_{NCG} is the NCG temperature, P_{NCG} is the NCG pressure and $\Re$ the ideal gas constant. The sub-index 0 refer to the working fluid charging conditions. Therefore, to estimate the length occupied by the NCG, the temperature and pressure must be determined.

The thermal circuit presented in Fig. 2c can be used to determine the NCG temperature. In this figure, T_v is the vapor temperature, R_{18} is the thermal resistance between the vapor (working fluid) and NCG, R_{14} is the wall conduction resistance, $h_{v\text{-}NCG}$ is the heat transfer coefficient between vapor and NCG, $h_{NCG\text{-}w}$ is the heat transfer coefficient between NCG and the tube wall and A_{NGC} is the internal area of the wall occupied by the NGC.

The NCG temperature is not significantly affected by the vapor temperature if the interface area between vapor and NCG is much smaller than the contact area of NCG with the tube. In other words,

Table 1
Order of magnitude of the thermal resistances (°C/W).

R_1 – evaporator external resistance (contact resistance experimentally obtained)	10^{-2}	1%
R_2 – evaporator radial wall conduction resistance	10^{-2}	1%
R_3 and R_4 – boiling resistances	10^{-2}	1%
R_5 – vapor resistance	10^{-7}	0%
R_6 and R_7 – condensation resistances	10^{-2}	1%
R_8 – condenser radial wall conduction resistance	10^{-2}	1%
R_{10} – axial wall conduction thermal resistance	10^{1}	0%
R_9 – condenser external resistance (through the calorimeter)	10^{0}	95%

in Fig. 2c, R_{19} is much smaller than R_{18}, and therefore, the NCG temperature tends to the external wall temperature. For this case, one can assume that $h_{v\text{-}NCG}$ is of the same order of magnitude of $h_{NCG\text{-}w}$. On the other hand, if the condenser length occupied by the NCG is small, the cross section and the NCG tube wall areas have the same order of magnitude and the NCG temperature turns to be very sensible to the heat transfer coefficients between vapor and NCG and NCG and wall. Also, the importance of the heat exchange by the tube lid area is increased. Therefore, in this case, a more precise model, which should consider the transition region between vapor and NCG, is much more complex and is not developed in this work. Actually, as it will be observed in Section 5, $h_{v\text{-}NCG}$ and $h_{NCG\text{-}w}$ will not be determined in the present work. Considering both R_{18} and R_{19}, from the thermal circuit of Fig. 2c, the NCG temperature is given by

$$T_{NCG} = T_v - R_{18}\frac{(T_v - T_{PC})}{(R_{18} + R_{19} + R_{14})} \tag{2}$$

Considering that the interface between NCG and vapor is static, the naphthalene and the NCG pressures must be equal. Therefore, the NCG pressures are obtained from saturated naphthalene property tables. Table 1 shows the order of magnitude of each resistance of the model presented in Fig. 2a and its contribution to the overall thermal resistance, for the thermosyphons tested in this work. One can note that the thermal resistances associated with axial heat conduction (R_{10}) are about 1000 times larger than the resistances associated with the working fluid. As these resistances are in parallel, the axial heat conduction resistances can be removed from the thermal circuit with negligible effect on the overall thermal resistance. The same observation can be made to resistance R_5, related to vapor pressure variations along the tube, negligible when compared with other resistances in series. Table 1 also shows that the thermal resistance between condenser external wall and the refrigeration liquid represents about 95% of the overall resistance.

4. Experimental setup

A well designed experimental apparatus should represent the actual operation conditions of the thermosyphon in industrial applications, where power inputs ranging from 5 to 50 kW/m^2 are usually found [14,20,21]. An efficient way to control the power input is controlling the heat delivered to the evaporator, by means of electrical resistances, for instance. On the other hand, the temperature levels should be controlled by the condenser heat output. Small heat exchangers (calorimeters), with temperature controlled water, are usually used for heat removal. The maximum operation temperature of these calorimeters is, for atmosphere open circuits, 100 °C. Therefore, to enable the use of thermal controlled baths to remove the heat from thermosyphons that operate at high temperatures (above 100 °C), it is suggested the introduction of an additional thermal resistance between thermosyphon and the cooling system. This effect can be obtained by a cavity filled with confined air.

Two different controls are used to determine the amount of the heat input and the temperature level of the device: the heat power input and the cooling thermal bath temperature. Fig. 3 shows a schematic of the heat removal system adopted in the present work, where the volume between the thermosyphon and the water reservoir is filled with air. Fig. 5a shows, in the right side, a view of the water jacket cooling calorimeter system and evaporator heating block. The heat is provided by means of four cartridge type electrical resistors of 0.4 Ω each, located inside a solid cylinder. A 25 kW power source (0–224 V, 0–10 A) is used in the heat generation. The voltage and the current are measured by means of a digital multimeter. Fig. 5b shows a schematic of the setup, with all the systems, including the heater, the cooler and the peripheral equipment employed. All tests were conducted in steady state conditions.

The temperature of the cooling water jacket is controlled by a thermal control bath that enters the calorimeter at 9 °C and leaves it at 50 °C, maximum. The water rate is measured by means of a 2 l beaker and a chronometer. Also, for comparison, the weight of the collected water is also measured using a 0.01 g precision weight meter. The calorimeter internal wall is made of a stainless steel AISI 316 tube, with external diameter of 38.4 mm and wall thickness of 1.5 mm. The gap formed between the thermosyphon wall and the heat meter internal wall is of 5 mm. Thermocouple wires are accommodated through this gap. The high thermal resistance observed through the air allows the temperature of the evaporator to reach the high levels required (~350 °C).

Cromel–Alumel, fiber glass covered thermocouples are used to monitor de temperatures. They are connected to the thermosyphon external wall by welding in the positions shown in Fig. 5a, left side: three in the evaporator, one in the adiabatic section and nine in the condenser section. In the adiabatic section and condenser, two thermocouples are installed for each axial position, in opposite radial locations. To improve the quality of the temperature measurements, the thermocouple reference junctions are connected to an insulated copper block inside a box (reference box), so that these junctions are isothermal. The temperature of the cooper block is compared with the temperature of the distillated water–ice bath, which temperature (zero Celsius degree) is checked using a high precision mercury thermometer. The thermocouples were calibrated by a calibration oven. The 95% uncertainty level of the temperature measurement is 0.2 °C, for temperature differences and 0.7 °C, for absolute temperatures.

To allow the thermocouple welding to the tube, a relatively thick thermocouple wire (0.7 mm) was used. For the evaporator region, where the temperatures are higher, conduction heat transfer through the thermocouple becomes important, affecting the temperature readings. Thermal grounding was obtained by thermally coupling small cooper tubes to the thermosyphon and making the thermocouple pass through them. The small tubes are not connected to the aluminum heating block and are considered isothermal. Therefore, the heat eventually conducted through the wires derives from these small tubes and not from the thermosyphon itself, avoiding temperature reading errors.

The condenser thermocouples were welded with 5 cm of distance. The junction was electrically insulated from the tube using sheets of mica and fiber-glass and thermally insulated (radiation) by means of the aluminum sheets. On the other hand, the condenser was coupled by radiation to the refrigeration system by black painting the external wall of the condenser tubes.

Care was taken to guarantee a good thermal insulation to the overall system. First, the adiabatic region was insulated by means of a thick rock wool. A wood box was constructed around the setup, which was filled with vermiculite.

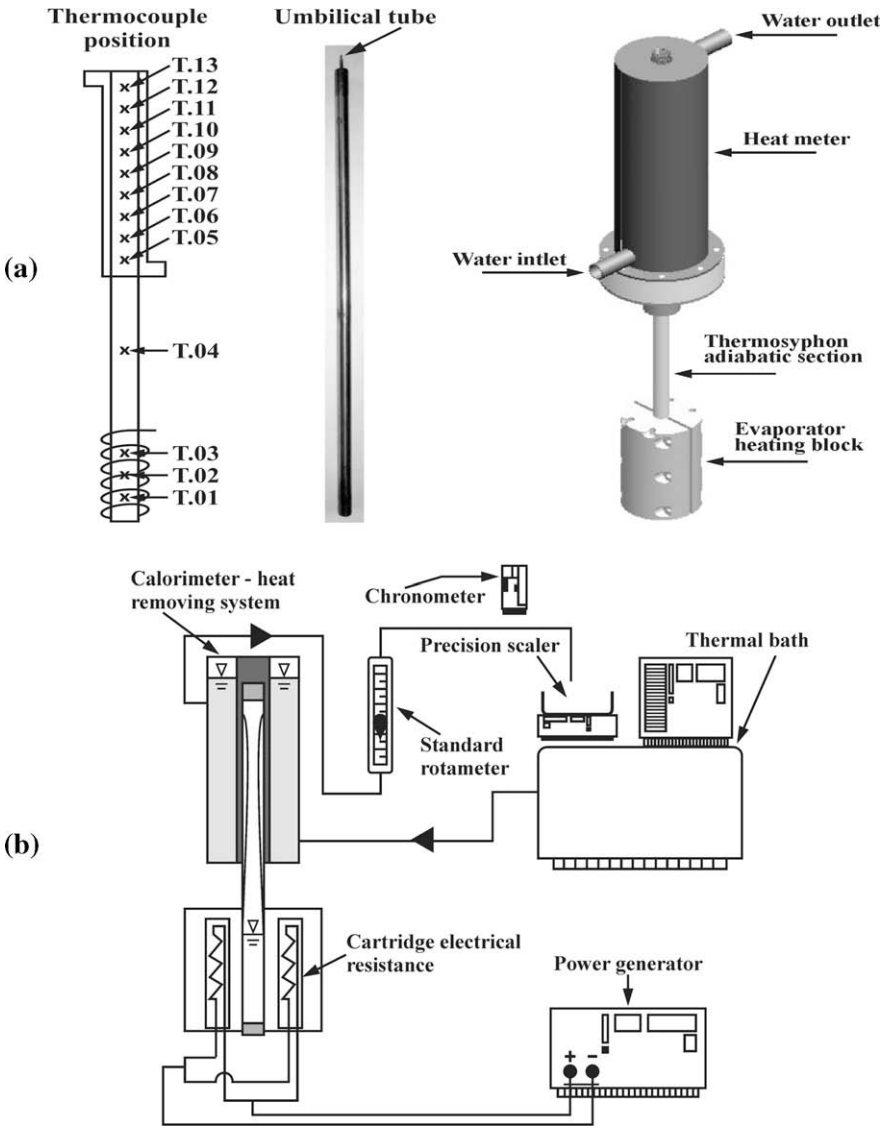

Fig. 5. Experimental apparatus. (a) Thermosyphon tested. (b) Schematic of the experimental setup, including peripheral equipment.

4.1. The naphthalene thermosyphon tested

A thermosyphon, made of stainless steel tubes and with naphthalene as working fluid, was designed, manufactured and tested in the laboratory. The NCG selected for the present study was argon. The thermosyphon casing is made of AISI 316, 25.4 mm external diameter tube, with 3 mm of wall thickness and 1 m of length. The closing lids are made from plates of the same material, using TIG (Tungsten Inert Gas) welding. The thermosyphon was divided into three sections: the evaporator, with 20 cm of length, an adiabatic section, 35 cm long, and a condenser section, of 45 cm of length. Following orientations of Pioro and Pioro (1997) [46] and the experience of the laboratory working group, the naphthalene was heated up to 90 °C before being charged to the thermosyphon. The valves and the charging (umbilical) tubing (see Fig. 5a), which connected the naphthalene reservoir to the tube, were also heated, to avoid that the naphthalene, solid in low temperature levels, to be trapped. Naphthalene (of 57.7 g) was introduced in the thermosyphon, which corresponds to 80% of the evaporator volume, considering the density of the naphthalene at 120 °C. The following charging procedure was adopted: by means of a vacuum pump, the air inside the tube was evacuated through the umbilical tube and a needle valve, until the pressure was below 10^{-2} Pa. This valve was closed and another needle valve, connected to the naphthalene (or to the argon) reservoir was opened. Due to the low pressure inside the tube, naphthalene (or argon) was sucked inside the tube, until the desired amount of naphthalene (or argon) was inputted to the tube. Some of the thermosyphons tested were purged after the working fluid charging. The purging procedure consists of opening the charging valve to remove gases from inside the thermosyphon when its internal pressure is above 1 atm. According to Table 2, five different charging configurations were adopted in the present study. The amount of NCG is controlled by means of the argon vessel pressure, when connected to the needle valve. Table 2 also provides the volume of the argon employed in three of the tested configurations. The mass of argon can be calculated using the ideal gas law, considering the pressure of the naphthalene vapor, given the operating temperature.

For the test configuration B thermosyphon (see Table 2), after a few operating hours and with the thermosyphon at 300 °C, the purging procedure was performed. The needle valve, connected to the upper regions of the condenser, is opened for about 3 s. At

Table 2
Charging configurations of the thermosyphons.

Test configuration	Test conditions	Volume (m^3) argon at 250 °C	Comments
A	No purge, no argon	0	Evacuated, charged with naphthalene
B	Purged, no argon	0	NCG eventually formed or left during charging procedure were removed
C	Purged, with argon at 2 bar, absolute pressure	9.119×10^{-5}	A purged tube is charged with argon at 2 bar, at room temperature
D	Purged, with argon at 3 bar, absolute pressure	10.220×10^{-5}	The 2 bar argon tube receives an extra argon charge of 3 bar
E	Purged, with argon at 11 bar, absolute pressure	16.51×10^{-5}	The 3 bar argon tube receives an extra argon charge of 11 bar

this temperature level, the thermosyphon internal pressure is higher than the atmosphere pressure and the NCG eventually formed or not eliminated during the charging procedure, is removed until a small amount of naphthalene is also eliminated. This procedure guarantees that the working fluid remaining is only naphthalene. The thermosyphon thermal performance in this configuration is very high. Therefore, the lower performance of the thermosyphon before purging, described as "no purge, no argon" test condition is credited to the remaining NCG. To study the influence of NCG, a controlled amount of argon, an inert gas, was inserted into the tube in three different amounts as described in the last three lines of Table 2.

5. Results

5.1. Condenser external resistance

Fig. 6a shows the theoretical external thermal resistance of the condenser as a function of the adiabatic section temperature, obtained from the model represented by the thermal circuit of Fig. 2a, which are compared with experimental data, for all cases listed in Table 2. The temperature of the adiabatic section is obtained from a thermocouple located at T04 position (see Fig. 5a), which represents the temperature level of the thermosyphon and is used as the naphthalene vapor temperature in the models.

From Fig. 6a, one can see that most of the points are next to the analytical result curve, shown in dashed line. Only two points, relative to the thermosyphon with a large amount of argon (configurations D and E bar) presented larger external thermal resistance than expected, when the system operates at temperature levels under 300 °C. For these cases, the amount of heat transferred is low, resulting in higher uncertainties in the heat measurements. In a general sense, the thermal circuit shown in Fig. 3 Detail A proved to be a good model for the prediction of the external condenser thermal resistance.

5.2. Evaporator internal resistance

Fig. 7a shows the results for the theoretical ($R_{int,evap}$ in Fig. 2b, right side) and experimental evaporator internal thermal resistance as a function of the adiabatic temperature, for all the tests listed in Table 2. As already mentioned, correlations from the literature were used for the estimation of the convection heat transfer in the evaporator section inside the thermosyphon. Most of the experimental points are located between the models that use the heat transfer correlations of Stephan and Abdelsalan and Foster and Zuber [24]. The highest thermal resistances were found for thermosyphons working with a large amount of NCG (configurations D and E, Table 2) for temperature levels under 300 °C. For low temperature levels, and therefore low pressures, the NCG

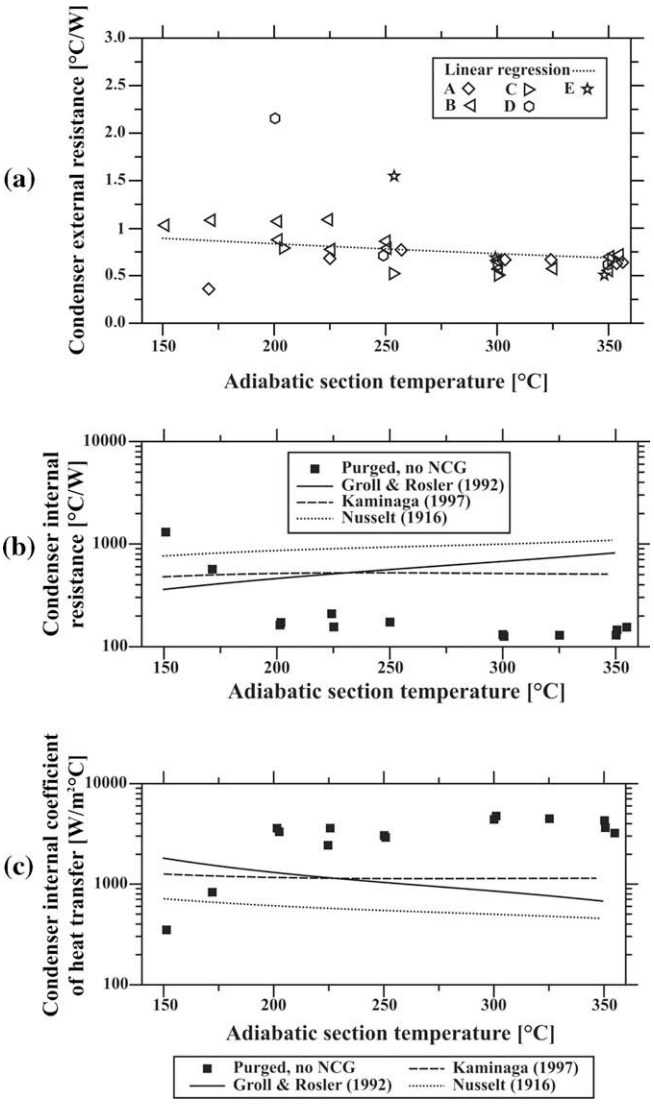

Fig. 6. Condenser thermal resistances and coefficients of heat transfer as a function of the adiabatic section temperature. (a) External resistances, all cases tested. (b) Theoretical and experimental internal thermal resistances, for configuration B. (c) Theoretical and experimental coefficients of heat transfer, for configuration B.

expand, occupying a large region of the condenser, affecting the performance of the whole device. One should remember that the model does not take into account any influence of the NCG in the evaporator region, which is considered completely full of the working fluid. The influence of the NCG in the condenser section will be presented later in this paper.

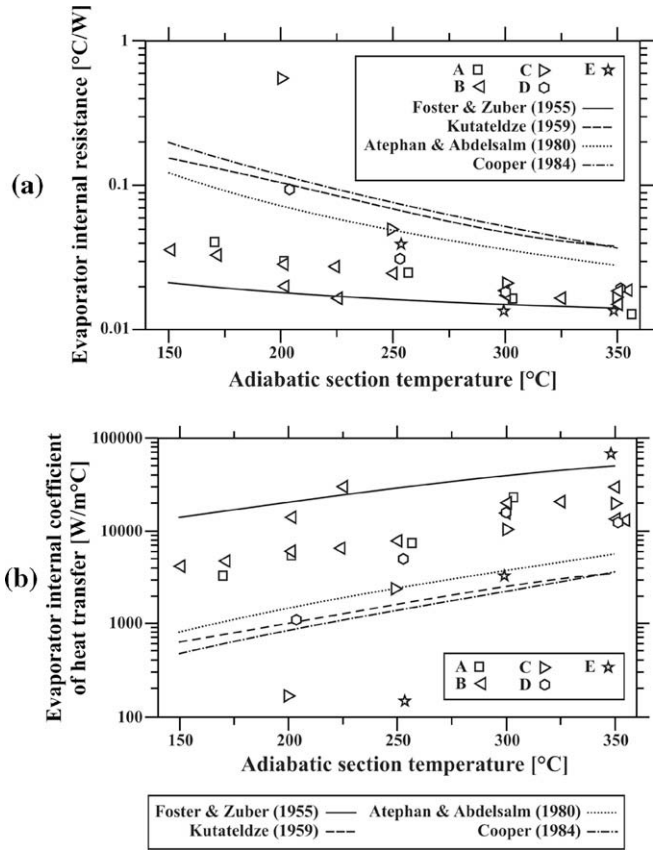

Fig. 7. Evaporator internal thermal resistances and coefficients of heat transfer as a function of the adiabatic section temperature for all models and data. (a) Thermal resistances. (b) Coefficients of heat transfer.

The evaporator internal coefficient of heat transfer can be obtained subtracting the wall heat conduction from the thermal resistance. The plot of this coefficient is shown in Fig. 7b. One can see from this figure that most of the data is between the curves obtained from the Stephan and Abdelsalan and Foster and Zubber, correlations, as observed in Fig. 7a. This is obvious, as the convection is the main resistance of the evaporator. It is interesting to note that, according to Bejan [41], the experimental values obtained for the coefficient of heat transfer lay within the range where most of the heat transfer coefficients of liquids, in boiling regime, are found, confirming that the boiling regime hypothesis is correct.

5.3. Condenser internal resistance

Fig. 6b presents the theoretical condenser internal resistance as a function of the adiabatic section temperature, which is compared with the data obtained for the thermosyphon test configuration B, according to Table 2. This configuration can be considered free of NCGand its data was selected for this comparison because the model used for the theoretical curves presented in this figure does not consider the presence of NCG. As already mentioned, three different literature correlations were used for the estimative of the heat transfer coefficients used in the theoretical models. One can note from this figure that the experimental thermal resistances are lower than the theoretical predictions, except for the low temperature data. One can also see that the best comparison is with the model which employs the Kaminaga correlation [25], considering both the temperature level and the curve trends (behavior of the resistance curve with the adiabatic section temperature).

Following the same procedure of the last section, the condenser internal heat transfer coefficient is obtained subtracting the wall radial conduction heat transfer from the thermal resistance, resulting in the curves presented in Fig. 6c. Again, in this case, the Kaminaga correlation showed the best comparison.

5.4. Effective length

To determine the tube effective length, the temperature distribution data is adjusted, by means of the Least Square Method, to a function, resulted from two superposed sigmoid (S shaped) functions, one relative to the region with no NCG (evaporator and part of condenser) and the other to the NCG condenser region. The sigmoid curve, in its most simple form, is [47]

$$y(x) = \frac{1}{(1+e^{x})} \tag{3}$$

The superposition of functions results in the temperature profile equation:

$$T(x) = \frac{T_{cond} - T_{NCG}}{1 + e^{\left(\frac{x - x_{v-NCG}}{s_{v-NCG}}\right)}} + \frac{T_{evap} - T_{cond}}{1 + e^{\left(\frac{x - x_{adiab}}{s_{adiab}}\right)}} \tag{4}$$

where T_{cond}, T_{NCG}, T_{evap} are the temperatures of the condenser, NCG and evaporator, respectively (obtained from the averages of the temperature data in these regions), $x_{v\text{-}NCG}$ and x_{adiab} are the positions of the interface vapor–NCG and of the adiabatic section and $s_{v\text{-}NCG}$ and s_{adiab} are parameters which rule the curve inclination in the concavity change point. A typical temperature distribution curve obtained from Eq. (4) is presented in Fig. 8a. The point of concavity change in the condenser is considered the NCG position, x_{NCG}. This data is employed in the thermal resistance models that consider the presence of NCG, which are compared with data, later in this work. This function presents and excellent comparison with data, as shown in Fig. 8b, for configuration A.

5.5. Temperature distribution

Fig. 8b shows the temperature distribution as a function of the thermosyphon length, where the position zero corresponds to the evaporator beginning and 100 cm to the condenser end, for the test configuration A (see Table 1), for several working temperature levels, in steady state conditions. The square points represent the temperature data, the full square symbols refer to the temperature of the adiabatic section. The test temperature was considered that of the adiabatic section, therefore, the maximum temperature for this test was 350 °C. As no purge is applied to the thermosyphon, NCG, resulting from some previous contamination of the working fluid and/or by insufficient vacuum in the tube before charging, are observed. Obviously, the NCG influence strongly the temperature distributions along the naphthalene thermosyphon, especially for lower temperature levels, as the NCG accumulate in the top region of the condenser. The NCG volume increases with the decrease of the internal pressure. From these curves, the effective length of the thermosyphon, important information for the design of heat exchangers, can be extracted from data, using Eq. (4) function. The diamond full symbol shows the effective length of the thermosyphon.

Fig. 8c shows the temperature distribution of configuration test B (see Table 2), which is equivalent to the same configuration of test A, after purging process. The data shows excellent temperature uniformity, especially for tube operating above 200 °C. For temperatures under this level, a temperature drop is observed, close to the condenser extremity. In this case, this temperature drop is attributed to the production of a low amount of vapor, which conden-

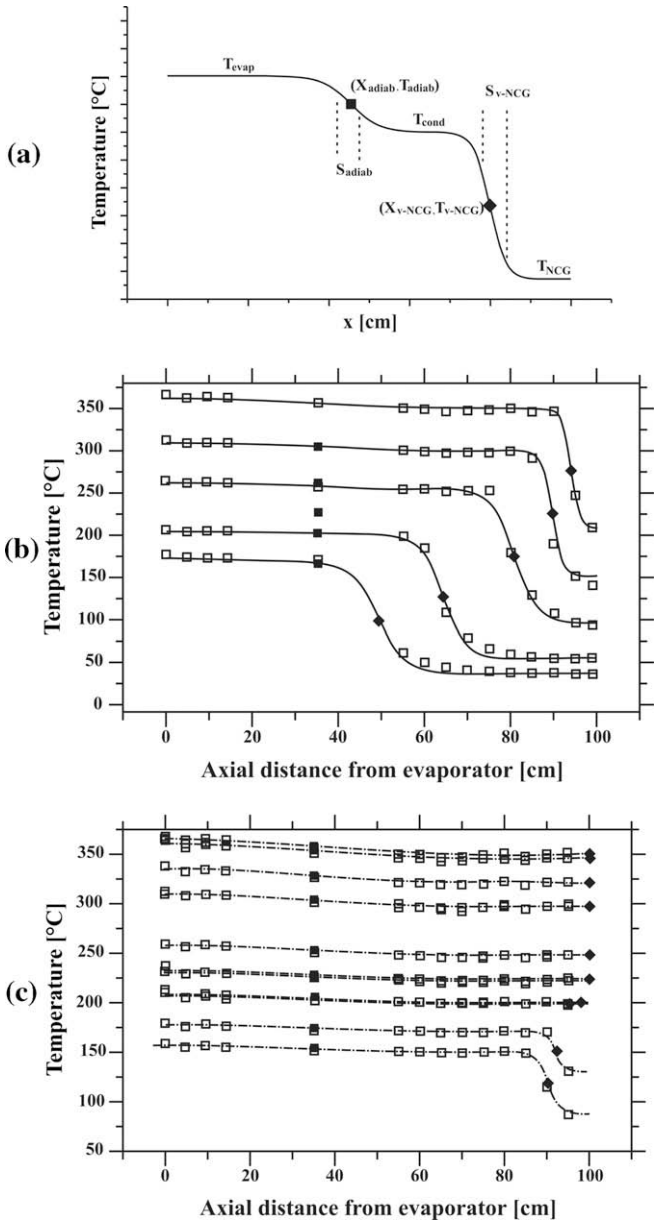

Fig. 8. Temperature distribution based in the superposition of two sigmoid curve models as function of the thermosyphon length. (a) Typical. (b) Experimental and sigmoid adjusted temperature curves (full line) for configuration A. (c) Experimental and sigmoid adjusted temperature curves (full line) for configuration B (purged, no argon).

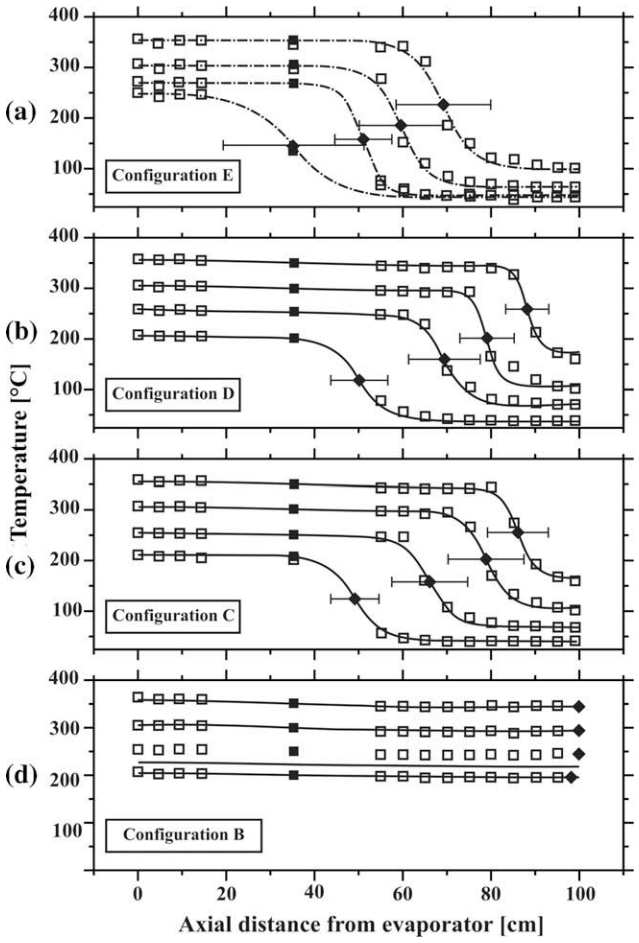

Fig. 9. Temperature distribution as a function of the thermosyphon length, for test configurations (see Table 1): (a) B, (b) C, (c) D and (d) E.

sates in a limited area of the condenser, decreasing the active length of the condenser.

Fig. 9 shows the temperature distribution for four configurations tested: (a) same configuration presented in Fig. 8c, (b) test configuration C, (c) test configuration D and (d) test configuration E. The same observations of Fig. 8c are also valid for this figure.

Fig. 10a presents the thermosyphon effective length as a function of the adiabatic section temperature for all the five configurations tested. The effective length is around the total length (100%) only for the free of NCG test configuration B, especially for higher working temperature levels. On the other hand, for configuration E and for low temperature levels, argon occupies all the condenser length, preventing the heat transfer. For the intermediate cases, (configurations C and D), the thermosyphon effective length is approximately the same and the device can still work properly for higher temperature levels. It is interesting to note that for high temperature levels, the naphthalene thermosyphon purge is not so important, as the configuration B (no purge, no argon) presents thermal behaviors only slightly better than the test configuration C.

The effective condenser length obtained from the configuration C (2 bar of argon) data is compared with the theoretical model, in Fig. 10b. The temperature of the NCG was not measured even though it was the input information for the determination of the effective length theoretical model. Therefore, two theoretical curves are presented: one considering the NCG temperature the same of the average condenser temperature (neglecting R_{18} and R_{19} in Fig. 2c thermal circuit) and the other considering the NCG temperature the same of the adiabatic section temperature (neglecting R_{18} and considering R_{19} very large, in Fig. 2c). Theoretically, the Fig. 10b hachured area between these two curves represents the region where the experimental data should lie. But this figure shows that both models under predict the effective length of the thermosyphon. This discrepancy may be attributed to the transition region between naphthalene vapor and NCG, considered flat in the model, while the temperature data (and the literature as well) suggests that this transition is smooth. The configuration C case was considered typical and the comparison of model with other data will not be presented in this work.

A glass tube naphthalene thermosyphon was constructed to visualize the two-phase flow inside the tube and it was observed an intense liquid drag by the vapor. The dragged liquid penetrates the NCG region, creating a mixing region, where some condensa-

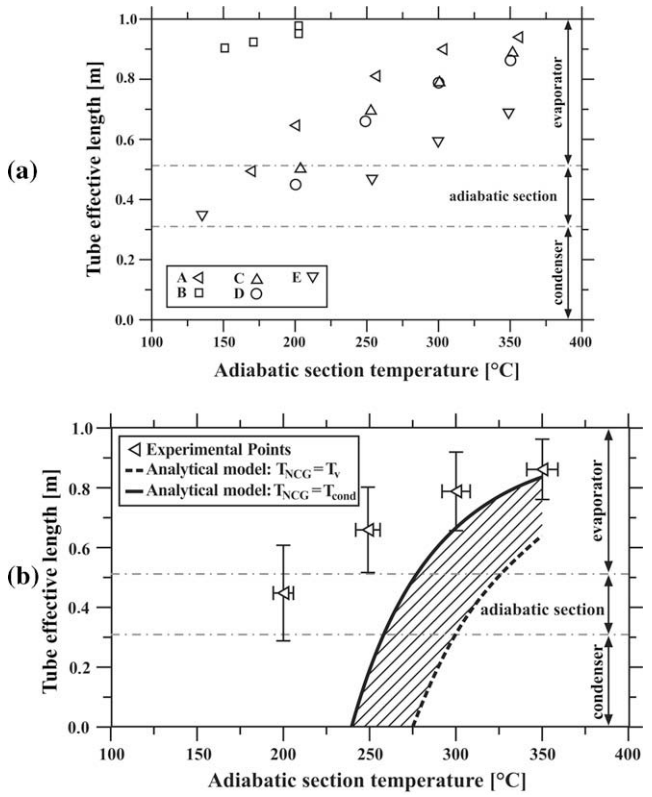

Fig. 10. Thermosyphon effective length as a function of the adiabatic section temperature. (a) Experimental, for all configurations presented in Table 1. (b) Theoretical and experimental for configuration C (2 bar).

tion is still verified. Actually, this dragging effect, together with the mass diffusion effects in the vapor/NCG transition region, increases the effective length of the thermosyphon. In this work, the mixing region was not modeled. Therefore, the theoretical model applied for the condenser internal thermal resistance with NGC was the same of the model applied for the NCG thermosyphon, considering the effective length of the condenser.

The experimental condenser thermal resistances are determined as the ratio between the temperature drop (between the condenser and the vapor temperatures) and the power input, for the effective length of the device. The temperatures used in the calculation of these resistances are obtained from the integration of the adjusted sigmoid temperature profile curve, over two different lengths: the total and the effective. Fig. 11 presents the experimental condenser thermal resistance as a function of the adiabatic section temperature for the total condenser length (square symbols) and for the effective length (circles), for the 2 bar case. As expected, the condenser resistances, considering the total length, are higher as part of the condensation area is inactive due to the presence of NCG.

5.6. Thermosyphon thermal resistance

In this section, the overall thermal resistance, defined as the ratio between the difference of temperatures of the evaporator and of the condenser walls and the heat power transferred through the thermosyphon, is presented. As already stated, the internal coefficients of heat transfer for the evaporator and for the condenser are input data for the thermal resistance model and are obtained from literature correlations. The experimental effective lengths are, in turn, used as input data for these correlations.

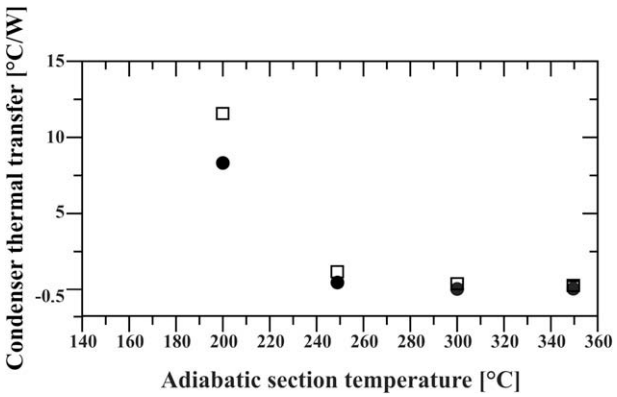

Fig. 11. Thermal resistances determined using the integral average of the sigmoid temperature profile curve, over the total (square symbols) and the effective (circles) condenser lengths, for the test configuration C.

Fig. 12a shows a comparison of the experimental thermal resistance for the test configuration B (no NCG, with purge) with the model, for all the combinations of correlations used for the estimative of the evaporator and condenser internal coefficients of heat transfer. From this plot one can see that the data always under predict the models, for temperature levels above 200 °C. For this temperature range, the best comparison is obtained using the thermal resistance model with the correlations of Groll and Rosler (condenser) and Foster and Zuber (evaporator). An average difference of around 51% is obtained, considering all experimental data; this

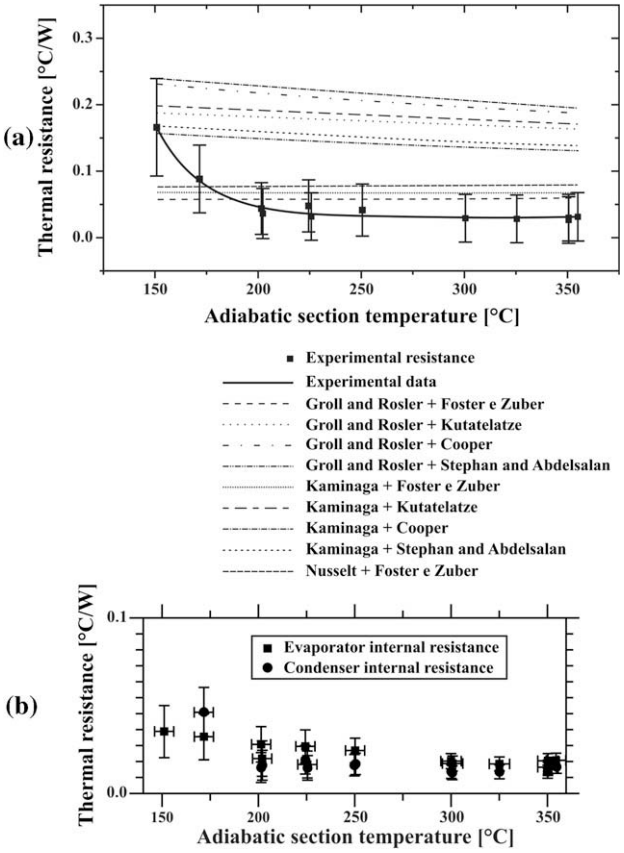

Fig. 12. Overall thermal resistance as a function of the adiabatic section temperature for configuration B (purged and no argon tube) data. (a) Comparison with models resulting from the combination of all literature correlations. (b) Experimental data and uncertainties observed.

difference drops to 38% if the data for the lowest temperature level is removed from the calculation. The lowest temperature data clearly do not follow the model trends. As the heat conduction models are very precise and as the thermophysical properties of steel (thermosyphon casing) are well known, one can conclude that the difference between data and model can be mainly attributed to the literature correlations employed or to the determination of the effective length. Actually, the comparison between data and model can be considered reasonable, especially if one remembers that the correlations employed in these models were not developed for naphthalene. If the external resistances were included in the model, the average difference between model and data would decrease very much, as the contribution of these external resistances is about 95% of the overall resistance (see Table 1).

As already mentioned, from Fig. 6b one can see that the best comparison of the condenser internal thermal resistance is obtained using Kaminaga's correlation for the estimative of the coefficient of heat transfer. On the other hand, the overall thermal resistances obtained using Groll and Rosler or Kaminaga (both for condenser), coupled with Foster and Zuber model (for evaporator), are very similar, as observed in Fig. 12a. Actually, the model with correlations of Groll and Rolser together with Foster and Zuber, adjusted better to the data distribution, and therefore these models are recommended for the prediction of the thermal behavior of the naphthalene thermosyphons without NCG.

A similar study was conducted for the configuration C thermosyphon, which data are compared with model obtained from all the combinations of correlations in Fig. 13a). The effective length was used in the correlations. One can see from this figure that both the model and data present a sharp increase in the thermal resistance as the temperature decreases, but the model is not able to capture exactly this variation. Actually, the largest differences between models and data are found in the low temperature levels and this difference decreases as the temperature level increases. For temperatures above 225 °C, all the models present a relative good comparison with data. A zoom, highlighting the higher temperature level data, is presented in Fig. 13b, where one can observe that, in this case, the models tend to under predict the data and that the best comparison is obtained for the combination of Nusselt correlation for evaporator and Cooper correlation for condenser. Fig. 13c presents the comparison of data with the model for two combinations of correlations: Groll and Rosler plus Foster and Zuber (the same of configuration B) and Nusselt plus Cooper. The percentage difference between model and data is around 145% for both models for the temperature level around 200 °C. For higher temperature levels, this difference is about 72% for the Groll and Rosler plus Foster and Zuber model and 13% for the Nusselt plus Cooper model. Actually, this last model lies within the data uncertainty as it was observed for the configuration B case (Fig. 12a).

Actually, the two phase flow physical phenomena observed are different for naphthalene thermosyphons with or without NCG and so are the models that compare better with the data.

It is believed that the model worse performance for thermosyphons operating at low temperature levels is due to the uncertainty in the determination of the effective length. As the length occupied by the NCG is large for these temperatures and the uncertainty of the model used for the determination of this length is also large, the uncertainty of the overall thermal resistance model increases. Actually, as naphthalene thermosyphons are designed to operate at higher temperature levels, these uncertainties are not expected to affect significantly the prediction of the thermal performance of the thermosyphon equipment. Furthermore, the thermosyphon external resistances are much larger than the internal resistances and these uncertainties are diluted when the overall thermal resistance is determined. Similar results were found for the other configurations tested in this work and they will not be presented.

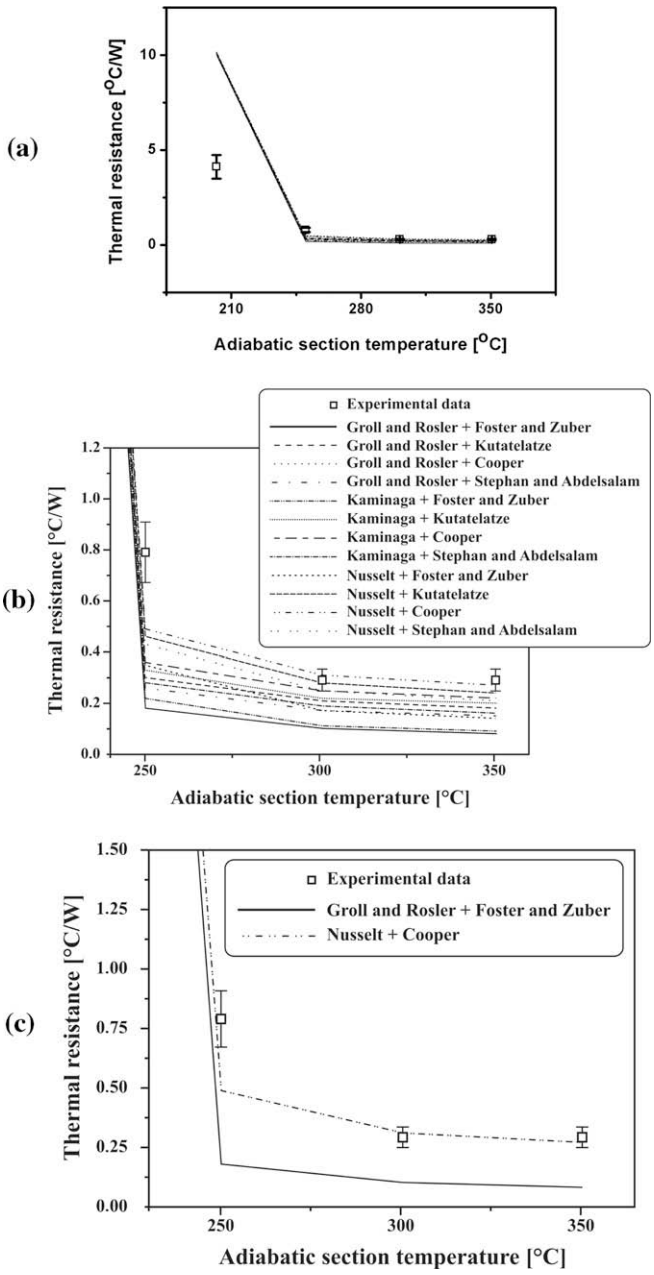

Fig. 13. Overall thermal resistance as a function of the adiabatic section temperature for test configuration C data (2 bar argon). (a) Theoretical results, for combinations of all literature correlations. (b) Zoom for low resistance region. (c) Comparison of data with Groll and Rosler plus Foster and Zuber and with Nusselt plus Cooper correlation models.

Concluding this section, one should note that the flat vapor–NCG interface model is precise enough for the determination of the overall thermal resistance of thermosyphon with or without NCG, and have been applied for the design of heat exchangers [20,21]. On the other hand, it should be emphasized that, if one needs more precise information about the thermal behavior of naphthalene thermosyphons, heat transfer correlations for the evaporation and condensation of this working fluid inside the thermosyphon must be carefully determined, or else, literature numerical 2D models can be employed.

5.7. Uncertainty analysis

The main sources of uncertainties observed in the experiment are due to the measurement of the temperatures and of the heat transferred by the tube. The maximum uncertainty observed for temperature differences is 1.3 °C in evaporator and 1.9 °C in condenser. The maximum uncertainty associated with the heat transfer rate is 24.12 W. This uncertainty is a combination of the uncertainties of the calorimeter temperatures of inlet and outlet refrigeration water and of the uncertainties in the measurement of the water mass flux. It represents around 5% of the maximum heat transfer rate used in purged thermosyphon experimental tests. Fig. 12b shows, in vertical bars, the uncertainties observed for the internal thermal resistances for the test configuration B (Table 1), as a function of the adiabatic section temperature. The uncertainties associated with the adiabatic section temperature measurements are represented in horizontal bars, in this same figure. This figure also shows that the better the system works, the lower are the associated uncertainties.

The uncertainties associated with the NCG thermosyphon are higher, especially for lower temperature levels. In this case, the NCG blocks a large region of the condenser, limiting the heat transferred and increasing the uncertainties associated with the location of the effective length of the tube. More details of the uncertainty analysis and of the experimental work, which data is employed for comparison in the present paper, is found in the work of Ângelo [42].

6. Conclusions

A naphthalene thermosyphon study was conducted in this paper. Although these devices has been employed in industrial heat exchangers that operates at temperatures above 250 °C, not much material is found in the literature about heat transfer modeling and data for naphthalene thermosyphons. Especial attention was given to modeling the thermal performance of naphthalene thermosyphons with NCG. A especial experimental setup, able to control the power input and the working temperature level of the device was designed, constructed and used in this work, to test a naphthalene thermosyphon, charged with different amounts of argon (NCG). This data was used for comparison with the modeling results. The experimental apparatus was also modeled and its thermal performance used in the analysis of the results.

It was observed that the presence of NCG deteriorates the thermal performance of the thermosyphon, as the NCG block the rear region of the condenser. This effect is more evident at the low temperature levels, as the NCG expand, occupying larger regions of the condenser. However, at high temperature levels, the naphthalene thermosyphon still works even with the presence of a considerable amount of NCG, which are compressed in small regions of the condenser not affecting very much the heat transfer capacity of the device. The purging process proved to be important, as NCG were observed during the thermosyphon operation, even when vacuum is provided before the working fluid charging.

To predict the thermal behavior of naphthalene thermosyphons, thermal circuit analogy models were developed. As no coefficient of heat transfer correlations based on naphthalene data are available, literature correlations were employed in this study. The several thermal resistances were individually determined theoretically and experimentally and compared with data. Therefore, information about the coefficients of heat transfer of the condensation and evaporation naphthalene process, useful for the design of this device, was collected.

Furthermore, the overall thermal resistance was also modeled and compared with data. At higher temperature levels, this comparison is better and so is the thermal performance of the device. From this study, the best combinations of literature correlations for the condensation and evaporation of naphthalene working fluids were selected. The model used for thermosyphons with or without NCG is basically the same, considering the effective length of the device. For the device operating without NCG in steady state conditions, the correlations of: Groll and Rosler (for the condenser internal coefficient of heat transfer) and Foster and Zuber (for evaporator), shown to be the best combination. On the other hand, for thermosyphons with NCG, the correlations of Nusselt (for condenser) and of Cooper (for evaporator) presented the best results.

As the naphthalene thermosyphons usually operates at high temperature levels (above 250 °C), where the precision of the model is good, the models developed can be considered good for heat exchanger design applications and are successfully implemented in software for the design of such equipment.

On the other hand, it is important to note that, if one needs precise information about the thermal behavior of naphthalene thermosyphons, correlations especially obtained for this working fluid or 2D numerical work must be developed.

Acknowledgements

The authors wish to acknowledge CNPq, for providing the Masters scholarship for the second author and Petrobras for financing this research.

References

[1] S. Lunay, V. Sartre, M.B.H. Mantelli, K.V. Paiva, M. Lallemand, Investigation of a wire plate micro heat pipe array, Int. J. Therm. Sci. 43 (2003) 499–507.
[2] M.B.H. Mantelli, K.V. Paiva, L.K. Longo, R. Gohr, V.B. Nicolau, Experimental tests of wire mini heat pipe under microgravity conditions aboard suborbital rockets, in: Proceedings of the 9th International Heat Pipe Symposium, Kuala Lumpur, Malaysia, 2008.
[3] K.V. Paiva, M.B.H. Mantelli, R. Gohr, M.A. Correa, Wire mini heat pipe under microgravity conditions, in: Proceedings of the 14th International Heat Pipe Conference (14th IHPC), Florianópolis, SC, 2007.
[4] F.H. Milanez, M.B.H. Mantelli, Thermal characteristics of a thermosyphon heated enclosure, Int. J. Therm. Sci. 45 (2006) 504–510.
[5] A.K. Silva, M.B.H. Mantelli, Thermal applicability of two phase thermosyphon in cooking chambers – experimental and theoretical analysis, Appl. Therm. Eng. 24 (2003) 717–733.
[6] M.B.H. Mantelli, F.H. Milanez, A loop thermosyphon for asphalt tank heating, in: Proceedings of the 8th International Heat Pipe Symposium, Kumamoto, Japan, 2006.
[7] P. Couto, J.M. Ochterbeck, M.B.H. Mantelli, Analysis of supercritical startup of cryogenic heat pipes with parasitic heat loads, J. Thermophys. Heat Transfer 19 (4) (2005) 497–508.
[8] P. Couto, M.B.H. Mantelli, J.M. Ochterbeck, Experimental analysis of supercritical startup of nitrogen/stainless steel cryogenic heat pipes, J. Thermophys. Heat Transfer 20 (4) (2006) 842–849.
[9] A.F.V. da Cunha, M.B.H. Mantelli, Analytical and experimental analysis of a high temperature mercury thermosyphon, J. Heat Transfer 131 (2009) 1–7.
[10] A.F.V. da Cunha, Análise de termossifões que operam a alta temperatura, D.Sc. Thesis, Federal University of Santa Catarina, Florianópolis, SC, 2008.
[11] P. Dunn, D. Reay, Heat Pipes, second ed., Pergamon Press, New York, 1978.
[12] L.L. Vasiliev, G.M. Volokhov, A.S. Gigevich, M.I. Rabetskii, Heat pipes based on naphthalene, J. Eng. Phys. Thermophys. 54 (1988) 623–626.
[13] D. Zhan, H. Zhang, Y. Liu, S. Li, J. Zhuang, Investigation of medium temperature heat pipe receiver used in parabolic through solar collector, in: Proceeding of the ISES World Congress, Beijing, China, 2007, vol.1, pp. 1823–1827.
[14] L.L. Vasiliev, Heat pipes in modern heat exchangers, Appl. Therm. Eng. 25 (2005) 1–19.
[15] G.P. Petersen, An Introduction to Heat Pipes: Modeling, Testing, and Applications, Wiley, New York, 1994.
[16] P.D. Dunn, D.A. Reay, Heat pipes, fourth ed., Pergamon Press, New York, 1994.
[17] S.W. Chi, Heat Pipe Theory and Practice a Sourcebook, Hemisphere, New York, 1976.
[18] A. Faghri, Heat Pipe Science and Technology, Taylor & Francis, London, 1995.
[19] S.H. Noie, Investigation of thermal performance of an air to air thermosyphon heat exchanger using ε-Nut method, Appl. Therm. Eng. 26 (2006) 559–567.
[20] D. Isoppo, T.P.F. Borges, M.B.H. Mantelli, Development of a detailed thermal model for designing heat pipe heat exchangers, in: Proceedings of the ECOS 2009, Foz do Iguaçu, Brazil, 2009.
[21] T.P.F. Borges, M.B.H. Mantelli, L.G. Persson, Techno-economic optimization of thermosyphon heat exchangers design using mathematical programming, in:

Proceedings of the 14th International Heat Pipe Conference, Florianópolis, SC, 2007.
[22] F. Incropera, D.P. De Witt, T.L. Bergman, A.S. Lavine, Fundamentals of Heat and Mass Transfer, sixth ed., Wiley, New York, 2007.
[23] M. Groll, S. Rösler, Operation principles and performance of heat pipes and closed two-phase thermosyphons, J. Non-Equilib. Thermodyn. 17 (1992) 91–151.
[24] M.B.H. Mantelli, R.D.M. Carvalho, S. Colle, D.U.C. Moraes, Study of closed two-phase thermosyphons for bakery oven applications, in: Proceedings of the 33th National Heat Transfer Conference, Albuquerque, New Mexico, 1999.
[25] J.G. Collier, J.R. Thome, Convective Boiling and Condensation, third ed., Oxford Science Publications, New York, 1996.
[26] U. Gross, Falling film evaporation inside a closed thermosyphon, in: Proceedings of the 8th International Heat Pipe Conference, Beijing, China, 1992.
[27] D.K. Edwards, B.D. Marcus, Heat and mass transfer in the vicinity of the vapor–gas front in a gas-loaded heat pipe, ASME J. Heat Transfer 94 (1972) 155–162.
[28] B.D. Marcus, G.L. Fleischman, Steady state and transient performance of hot reservoir gas controlled heat pipes, ASME paper no. 70-HT/SpT-11, 1970.
[29] A.R. Rohani, C.L. Tien, Steady two-dimensional heat and mass transfer in the vapor–gas region of a gas loaded heat pipe, ASME J. Heat Transfer 95 (1973) 377–382.
[30] K. Hijikata, S.J. Chen, C.L. Tien, Non-condensable gas effect on condensation in a two-phase closed thermosyphon, Int. J. Heat Mass Transfer 27 (1984) 1319–1325.
[31] P.F. Peterson, C.L. Tien, Gas-concentration measurements and analysis for gas-loaded thermosyphons, ASME J. Heat Transfer 110 (1988) 743–747.
[32] P.F. Peterson, C.L. Tien, Numerical and analytical solutions for two-dimensional gas distribution in gas-loaded heat pipes, ASME J. Heat Transfer 111 (1989) 598–604.
[33] L. Juxing, X. Tongming, A study on the property of heat and mass transfer of a gas-loaded thermosyphon, in: Proceedings of the 8th International Heat Pipe Conference, Beijing, China, 1992.
[34] S. Maezawa, K. Gi, H. Ishihara, Thermal characteristics of gas-loaded two-phase closed thermosyphon with gas reservoir, in: Proceeding of the 4th International Heat Pipe Symposium, Tsukuba, Japan, 1994.
[35] X. Zhou, R.E. Collins, Condensation in a gas-loaded thermosyphon, Int. J. Heat Mass Transfer 38 (1995) 1605–1617.
[36] H. Hashimoro, F. Kaminaga, K. Matsumura, Study on condensation heat transfer characteristics in a thermosyphon with non-condensable gas effect, in: Proceedings of the 11th International Heat Pipe Conference, Tokio, Japan, 1999.
[37] P. Kaiping, U. Renz, Thermal diffusion effects in turbulent partial condensation, Int. J. Heat Mass Transfer 34 (1991) 2629–2639.
[38] R.M. Bruce, L. Haber, P. McLure, Toxicological review of naphthalene, U.S. Environmental Protection Agency, Washington, 1998.
[39] A. Devarakonda, W.G. Anderson, Thermo-physical properties of intermediate temperature heat pipe fluids, in: Proceedings of the Space Technology and Applications International Forum (STAIF–2005), Albuquerque, NM, USA, 2005.
[40] W. Anderson, Intermediate temperature fluids for heat pipes and loop heat pipes, in: Proceedings of the International Energy Conversion Engineering Conference, St. Louis, MO, 2007.
[41] A. Bejan, Convective Heat Transfer, Wiley, New York, 1995.
[42] Angelo, W. B., Caracterização Térmica de um Termossifão Bifásico de Naftaleno, Msc Dissertation, Mechanical Engineering Department, Federal University of Santa Catarina, Brazil, 2007.
[43] M. Kamil, M. Shamsuzzoha, S.S. Alam, Effect of submergence on boiling incipience in a vertical thermosyphon reboiler, Int. J. Therm. Sci. 44 (1) (2005).
[44] K. Stephan, M. Abdelsalam, Heat-transfer correlations for natural convection boiling, Int. J. Heat Mass Transfer 23 (1) (1980) 73–87.
[45] M.G. Cooper, Saturation nucleate boiling: a simple correlation, in: Proceedings of the International Chemical Engineering Symposium Series, 1984 pp. 785–793.
[46] L.S. Pioro, I.L. Pioro, Industrial Two-phase Thermosyphons, Begell House, New York, 1997.
[47] F.K. Hoehler, Logistic equations in the analysis of S-shaped curves, Comput. Biol. Med. 25 (3) (1995) 367–371.